THE JOURNAL OF PHYSICAL CHEMISTRY A

pubs.acs.org/JPCA Article

Highly Conjugated, Fused-Ring, Quadrupolar Organic Chromophores with Large Two-Photon Absorption Cross-Sections in the Near-Infrared

Taylor G. Allen, Sepehr Benis, Natalia Munera, Junxiang Zhang, Shuixing Dai, Tengfei Li, Boyu Jia, Wei Wang, Stephen Barlow, David J. Hagan, Eric W. Van Stryland, Xiaowei Zhan, Joseph W. Perry,* and Seth R. Marder*

Cite This: https://dx.doi.org/10.1021/acs.jpca.0c02572 Read Online

ACCESS | Metrics & More | Article Recommendations | Supporting Information

ABSTRACT: The two-photon absorption (2PA) properties are investigated for two series of organic, π-conjugated, fused-ring, quadrupolar A-π-D-π-A chromophores of the type originally developed as nonfullerene acceptors for organic photovoltaics. These molecules are found to exhibit large nondegenerate two-photon absorption (ND2PA) cross-sections (ca. 6−27 $\times 10^3$ GM) in the near-infrared (NIR). In the first series, involving molecules of varying core size, ND2PA spectra and cross-sections characterized by femtosecond ND2PA spectroscopy in chloroform solutions reveal that increases in core size, and thus conjugation length, leads to substantially red-shifted and enhanced 2PA. In a second series, variation of the strength of the terminal acceptor (A) with constant core size (seven rings, indacene-based) led to less dramatic variation in the 2PA properties. Among the two core types studied, compounds in which the donor has a thieno[3,2-*b*]thiophene center demonstrate larger 2PA cross-sections than their indacene-centered counterparts, due to the greater electron-richness of their cores amplifying intramolecular charge transfer. Excited-state absorption (ESA) contributions to nonlinear absorption measured by open-aperture Z-scans are deduced for some of the compounds by analyzing the spectral overlap between 2PA bands and NIR ESA transitions obtained by ND2PA and transient absorption measurements, respectively. ESA cross-sections extracted from transient absorption and irradiance-dependent open-aperture Z-scans are in reasonable agreement, and their moderate magnitudes (ca. 10^{-21} m^2) suggest that, although ESA contributions are non-negligible, the effective response is predominantly instantaneous 2PA.

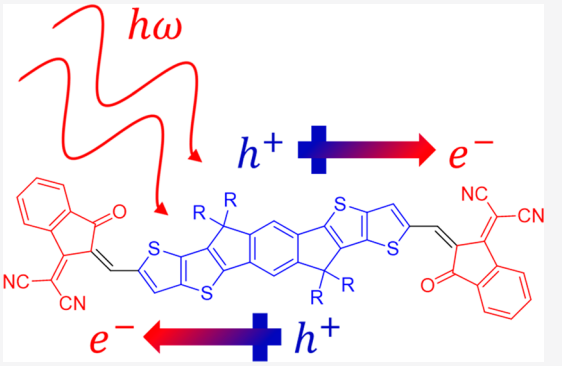

INTRODUCTION

Materials exhibiting efficient two-photon absorption (2PA) have been used for a variety of applications such as biological imaging,[1] microfabrication,[2] optical-limiting,[3] and three-dimensional optical data storage.[4] The success of these pursuits can largely be attributed to substantial efforts in material design by which the efficiency and spectral range of a 2PA material can be optimized. In this regard, organic materials offer many advantages due to the wealth of synthetic chemistries available to tune the structures of a variety of π-conjugated molecules and polymers whose electronic structure are conducive to large 2PA responses.[5,6] In particular, quadrupolar molecules with highly delocalized π-systems have drawn considerable attention due to the substantial 2PA enhancements that can be derived through judicious changes in their structure.

The cross-sections for excitation into the 2PA-allowed states of quadrupolar molecules (e′, Figure 1) benefit from strong coupling with the intermediate one-photon-allowed state (e, Figure 1) and the associated transition dipole moments (TDMs) contributing to the overall quadrupolar polarization upon excitation.[7,8] As derived from an essential states model, these contributions to the nondegenerate 2PA (ND2PA) cross-section (δ) are described by a quadratic dependence (eq 1) on both the g → e (M_{ge}) and e → e′ ($M_{ee'}$) TDMs, where Γ_{ge} is the damping term for the one-photon absorption (1PA) transition (g → e) and, $E_{ge} - \hbar\omega_1$ and $E_{ge} - \hbar\omega_2$ are detuning energies between the 1PA transition energy (g → e, E_{ge}) and the energies of the two nondegenerate photons completing the ND2PA transition (g → e′, Figure 1 right-most transition). K is a prefactor which, as shown in eq 2, is a function of the refractive indices of the medium, n_1 and n_2, at frequencies ω_1 and ω_2, respectively, and also incorporates constants including

Received: March 23, 2020
Revised: May 2, 2020
Published: May 7, 2020

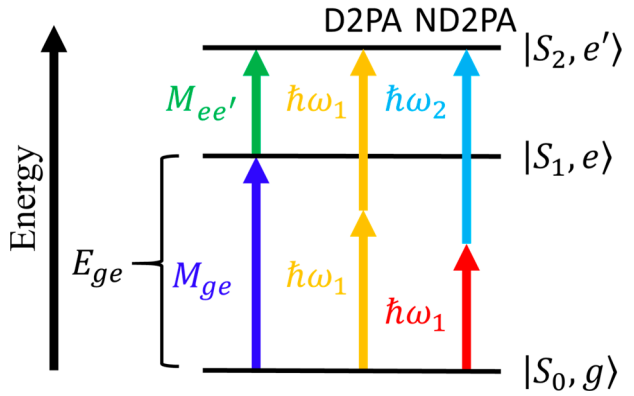

Figure 1. Jabłoński diagram for quadrupolar molecules showing the quantities involved in degenerate two-photon absorption (D2PA) and nondegenerate two-photon absorption (ND2PA) into a 2PA-allowed state, S_2, where S_1 is a 1PA-allowed state, as described by an essential-states model.

the speed of light (c) and vacuum permittivity (ε_0).[7−9] L_1 and L_2 are the Lorentz local field factors given by, $L_i = (n_i^2 + 2)/3$.

$$\delta \approx K \frac{M_{ge}^2 M_{ee'}^2}{\Gamma_{ge}} \left(\frac{1}{E_{ge} - \hbar\omega_1} + \frac{1}{E_{ge} - \hbar\omega_2} \right)^2 \quad (1)$$

$$K = \frac{3L_1^2 L_2^2}{5n_1 n_2 c^2 \epsilon_0^2 \hbar} \frac{\hbar\omega_2 (\hbar\omega_1)^2}{(\hbar\omega_1 + \hbar\omega_2)} \quad (2)$$

Several classes of D-A-D and D-π-A-π-D (where D and A represent electron-donating and -accepting groups, respectively, and π represents extended conjugation) quadrupolar dyes have exhibited large 2PA when the strengths of the D and A moieties are appropriately tuned.[10−13] Compounds with sizable 2PA in the 1200−1600 nm range of the near-infrared (NIR) are of interest for various applications such as biomedical imaging and photon upconversion for photodynamic therapy and energy conversion.[14−16] The number of studies of 2PA at wavelengths of 1000−1600 nm are more limited than those with large 2PA in the visible or short-wave IR (ca. 500−1000 nm); however, examples include: a few D-A-D/D-π-A-π-D quadrupolar chromphores including extended squaraines,[17] porphyrin-substituted squaraines,[18] and extended oligo(arylenevinylene) derivatives;[19,20] dipolar organic chromophores;[21] metal−organic compounds such as nickel bis(dithiolene) complexes;[22] dimeric porphyrin derivatives,[6,23,24] porphyrin polymers,[25] phthalocyanines;[6,26] and BODIPY boron derivatives.[27] Other approaches that have enabled large nonlinear absorption in this wavelength range include europium(III)-containing metal−organic frameworks[28] and nanoparticles,[29] and plasmon-assisted 2PA enhancements in silver nanoparticles coated with organic materials.[30]

Recently, organic A-π-D-π-A fused-ring compounds have been reported as alternative electron acceptors to fullerenes in organic photovoltaics and have led to substantial gains in photovoltaic efficiency in bulk-heterojunction blends.[31−34] The structural motifs of these materials are, however, also promising for 2PA because they possess highly delocalized π-systems with rigid, planar, electron-rich cores and in-plane electronic coupling to acceptor groups at the periphery of the molecule. Specifically, examples that exhibit strong, long-wavelength (ca. 700−1000 nm) 1PA are potential candidates to exhibit large 2PA further into the NIR. As shown in the literature,[35,36] the optical properties of compounds with π-conjugated fused rings are heavily influenced by changes in the geometry, functionalization, planarity, and size of these moieties. The aforementioned fused-ring photovoltaic acceptors allow straightforward extension of effective conjugation by increases in the length of the central fused-ring π-core without introducing conformational degrees of freedom that disrupt conjugation. Additionally, the acceptor (A) strength can be tuned to modulate the degree of quadrupolar charge transfer in the excited states relative to the ground state.[6] In doing so, one can efficiently extend 2PA and 1PA to longer wavelengths and potentially enhance the magnitude of 2PA in the NIR due to smaller detuning energies.

The focus of this study is to understand key structure−property relationships that govern the 2PA response for a set of

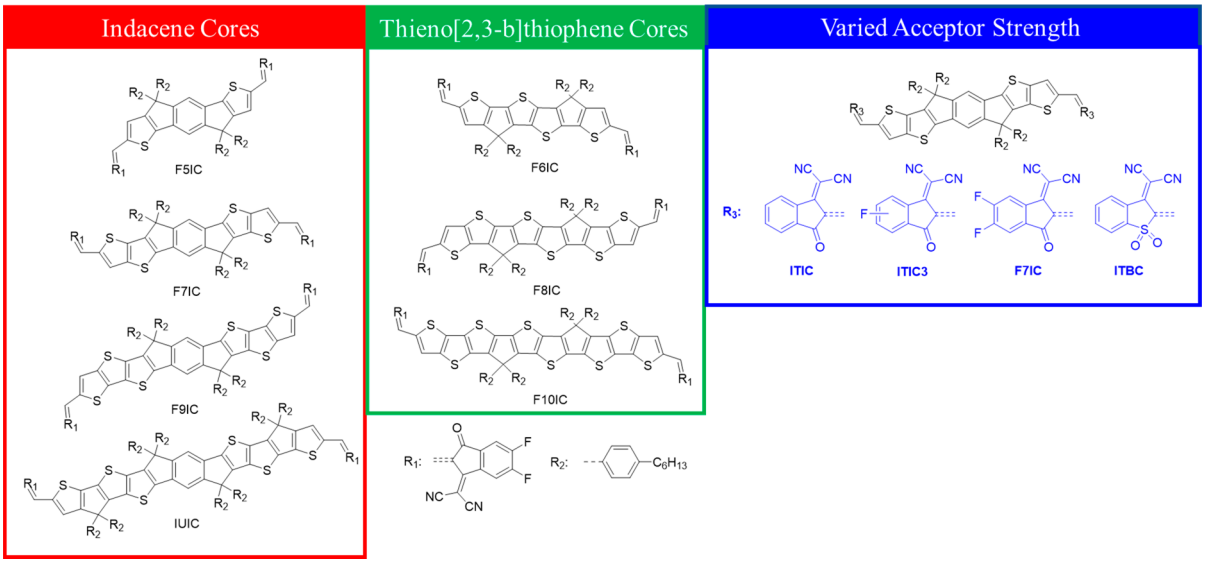

Figure 2. Structures of varied-cored indacene (red) and thieno[2,3-*b*]thiophene (TT, green) compounds and indacene compounds with varied acceptors (blue).

https://dx.doi.org/10.1021/acs.jpca.0c02572
J. Phys. Chem. A XXXX, XXX, XXX−XXX

A-π-D-π-A chromophores (Figure 2) of the type developed for photovoltaic applications, with planar, electron-rich, fused-ring cores and strong electron-withdrawing terminal groups. First, 2PA magnitudes and spectral trends are measured and discussed as a function of D core size (i.e., conjugation length) via the incremental addition of fused thiophene rings to indacene- and thieno[3,2-*b*]thiophene (TT)-based cores while keeping the terminal acceptor constant. Second, the extent to which 2PA enhancements can be derived from changes in acceptor strength for a constant core size (in our case, a seven-ring indacene-based core) will be examined.

In this investigation, femtosecond ND2PA spectroscopy (ND2PAS) is used to simultaneously obtain changes in ND2PA spectra and their respective magnitudes for all compounds (Figure 2) in chloroform solutions. Excited-state absorption (ESA) contributions to nonlinear absorption are characterized by femtosecond transient absorption (TA) spectroscopy and open aperture (OA) Z-scans[37] at 1200 and 1300 nm, all in chloroform solution. Based on these measurements, analysis is provided regarding the molecular origin of 2PA enhancements that are the result of amplified intramolecular charge transfer described by an essential-states model.

EXPERIMENTAL METHODS

Synthetic Details. The compounds were synthesized according to the literature: **F5-9IC**,[32] **IUIC**,[38] **F6-10IC**,[33] **ITIC**,[31] **ITIC3**,[34] and **ITBC**.[39]

Steady-State Absorption Spectroscopy. UV−vis-NIR measurements were performed on a Shimadzu UV3101-PC dual arm spectrometer using 1 cm quartz cuvettes. All solutions were made using spectrophotometric grade chloroform (J.T. Baker 9175-02), and concentrations were within a range of ca. 1−10 μM.

Femtosecond Transient and Nondegenerate Two-Photon Absorption Spectroscopy. Femtosecond TA[40] and ND2PAS[41] measurements were performed using a commercial pump−probe system (Helios, Ultrafast Systems) in a noncollinear geometry. The pump source was a TOPAS-C optical parametric amplifier (tunable output from ca. 450−2800 nm) pumped at 795 nm by a regeneratively amplified laser system (Solstice, SpectraPhysics) with ∼100 fs HW1/e pulse widths and 1 kHz repetition rate. The pump beam was chopped to 500 Hz. Typical 1/*e* diameters for the Gaussian pump beams used in ND2PAS and TA were 500 μm. Typical Gaussian visible (spectral range ca. 420−760 nm) NIR (spectral range ca. 830−1600 nm) white light probe 1/*e* diameters were 100 and 200 μm, respectively. For TA and ND2PAS a range of pump energies from ca. 2−16 μJ was used, depending on the response of the sample and to check for abnormal fluence-dependent responses. ND2PA spectra were acquired using pump wavelengths of 1300 and 1550 nm, and repeatable ND2PA cross-sections were obtained for most compounds. For some compounds (**F8IC**, **F10IC**, and **IUIC**), 1300 nm was close to the degenerate 2PA frequency, and, therefore, all spectra and cross-sections reported here were acquired by pumping at 1550 nm, which avoided degenerate pumping and enabled the observation of ND2PA transitions for all compounds in the available NIR white-light window. ESA cross-sections for all compounds were characterized using the TA ground-state depletion method.[40] All samples were pumped at 720 nm, and the extinction coefficient of the ground-state bleach signal at 680 nm for all compounds except **F8IC**, **F10IC**, and **IUIC** (715 nm used instead due to low absorbance at 680 nm) was used for calculating ESA cross-sections. All measurements were made using spectrophotometric grade chloroform (J.T. Baker 9175-02) and 2 mm quartz cuvettes while stirring. Concentrations used for ND2PAS and TA were ca. 1 mM and ca. 0.01−0.05 mM, respectively. Each TA and ND2PA spectrum was processed to correct for solvent background, pump scattering, and probe chirp using Surface Xplorer (Ultrafast Systems) prior to analysis. ND2PA and ESA cross-sections were calculated using MATLAB. ND2PA spectra shown in Figure 4a,b and Figure 7a are plotted in terms of transition wavelength (λ_{trans}), defined in eq 3, where λ_e and λ_p are pump and probe wavelengths, respectively. The equivalent laser wavelength is given on the top *x*-axis, which is double the transition wavelength.

$$\lambda_{trans} = \left(\frac{1}{\lambda_e} + \frac{1}{\lambda_p}\right)^{-1} \tag{3}$$

In the case of ND2PA and ESA, the induced changes in probe irradiance can be formulated as

$$\frac{dI_p}{dz} = -2\alpha_2^{ND} I_e I_p - \sigma_{ESA} N_{ex} I_p \tag{4}$$

where α_2^{ND} is the ND2PA absorption coefficient, N_{ex} is the number density of the excited molecules, σ_{ESA} is the ESA cross-section, and I_p and I_e are the probe and pump irradiances, respectively. With excitation at 1550 nm, we keep the irradiance sufficiently low that there is negligible generation of excited states via D2PA of the excitation pulse, i.e., N_{ex} is negligible and ESA may be neglected. Then the only mechanism contributing to nonlinear absorption is ND2PA. For the characterization of molecular systems, it is convenient to define the 2PA cross-section as $\delta_2^{ND} = \alpha_2^{ND}\hbar\omega_p/N$, where N is the total molecular density. The commonly used units for 2PA cross-sections are Goeppert−Meyers (GM), where 1 GM = 10^{-50} cm^4·s·photon^{-1}.

In the case of TA measurements pumping with 720 nm, where the pump generates excited states via linear absorption, the governing equations are

$$\frac{dI_p}{dz} = -\sigma_{ESA} N_{ex} I_p \tag{5}$$

$$\frac{dN_{ex}}{dt} = \frac{\alpha_e I_e}{\hbar\omega_e} \tag{6}$$

with $\hbar$ is the reduced Planck constant, α_e is the linear absorption coefficient at the pump wavelength, and ω_e is the angular frequency of the pump. In this case, ESA dominates over any nondegenerate 2PA.

Femtosecond Single-Arm Open-Aperture Z-scan. For degenerate Z-scans in the near IR, we must consider both 2PA and ESA as nonlinear absorption mechanisms, in which case the change in irradiance, I, is given by

$$\frac{dI}{dz} = -\alpha_2^{D} I^2 - \sigma_{ESA} N_{ex} I \tag{7}$$

$$\frac{dN_{ex}}{dt} = \frac{\alpha_2^{D} I^2}{2\hbar\omega} \tag{8}$$

where α_2^D is the D2PA coefficient. The degenerate 2PA cross-section, $\delta_2^D = \alpha_2^D\hbar\omega/N$. As N_{ex} is proportional to I^2, ESA is a

https://dx.doi.org/10.1021/acs.jpca.0c02572
J. Phys. Chem. A XXXX, XXX, XXX−XXX

higher order process, so the 2PA coefficient may be fit for lower energy Z-scans, and the ESA cross-section may be subsequently determined from higher energy data. Alternatively, we may ascribe an effective 2PA cross-section,

$$\delta_2^{\text{eff}} = \delta_2^{\text{D}} + \sqrt{\frac{\pi}{2}} \frac{\sigma_{\text{ESA}} \delta_2^{D} \lambda}{8\pi\hbar c} \frac{\tau_{\text{FWHM}}}{\sqrt{\ln(2)}} I \quad (9)$$

which can simply be fit to the transmittance at focus.[42,43] τ_{FWHM} is the FWHM pulse width.[44] Plotting the δ_2^{eff} versus irradiance allows quick determination of both δ_2^{D} and σ_{ESA} from the intercept and the slope of the plot, respectively. We attempted both approaches and obtained close results.

For the experiment, a regeneratively amplified Ti:sapphire laser system (Clark-MXR) with ∼150 fs HW1/eM pulse widths and 1 kHz repetition rate was used to pump an optical parametric amplifier (TOPAS-C OPA) to generate a signal beam at wavelengths of 1200 and 1300 nm. Measurement wavelengths for each compound were chosen based on the 2PA response at that wavelength found by ND2PA. For **F9IC** and **IUIC**, measurements were performed at 1200 and 1300 nm. The signal beam was spatially filtered to obtain a Gaussian beam profile and aligned to the OA Z-scan setup. A thin piece of GaAs (0.625 mm) was used to calibrate the setup and to characterize the beam size at the focus, and the exact pulse width at each wavelength was measured via second-order autocorrelation. All measurements were made in 1 mm quartz cuvettes in solution with spectrophotometric grade chloroform (chloroform, 99.8%, spectroscopy grade, stabilized with ethanol, ACROS Organics).

RESULTS AND DISCUSSION

Influence of Core Size on One- and Two-Photon Absorption. *One-Photon Absorption.* Normalized 1PA spectra in dilute chloroform solutions (ca. 6−10 μM) are plotted in Figure 3a,b showing 1PA spectral changes as a function of core size. For the indacene- and TT-based series, an increase in ring count results in red-shifted 1PA peaks ($\lambda_{\text{max}}^{\text{1PA}}$); this has generally been ascribed largely to increasing destabilization of the primarily core-based HOMO, the LUMO being more localized on the terminal groups and less sensitive to core size.[32,33] For the indacene-based compounds (Figure 3a), $\lambda_{\text{max}}^{\text{1PA}}$ values were found to steadily increase by ca. 20 nm in the order of **F5IC** < **F7IC** < **F9IC** but then dramatically increase by 64 nm between **F9IC** and **IUIC**. It is worth noting, however, that from **F5IC** to **F7IC** to **F9IC**, increasing numbers of thiophene rings are fused to the indacene, whereas **IUIC** has the same number of thiophene rings as **F9IC** and differs in having an additional cyclopentadiene ring inserted into each fused-thiophene portion of the molecule. The spectral width increases modestly with the number of rings in the series **F5IC**−**F9IC** (1PA full width at half-maximum, Γ_{ge} = 154, 226, 234 meV, respectively), while **IUIC** is an exception (176 meV), clearly due to the reduction in the high-energy shoulder adjacent to the primary absorption band for **IUIC** compared to that seen for other compounds with fewer rings, which is likely related to changes in vibrational fine structure.[38] Absorption spectra for the TT series (Figure 3b) gave a similar trend; however, all dyes from this set absorbed at longer wavelengths compared to indacene dyes with cores even one ring larger. This has previously been attributed to a destabilized HOMO and stabilized LUMO for TT dyes relative to indacene dyes.[34,45] Similar degrees of spectral broadening were found for

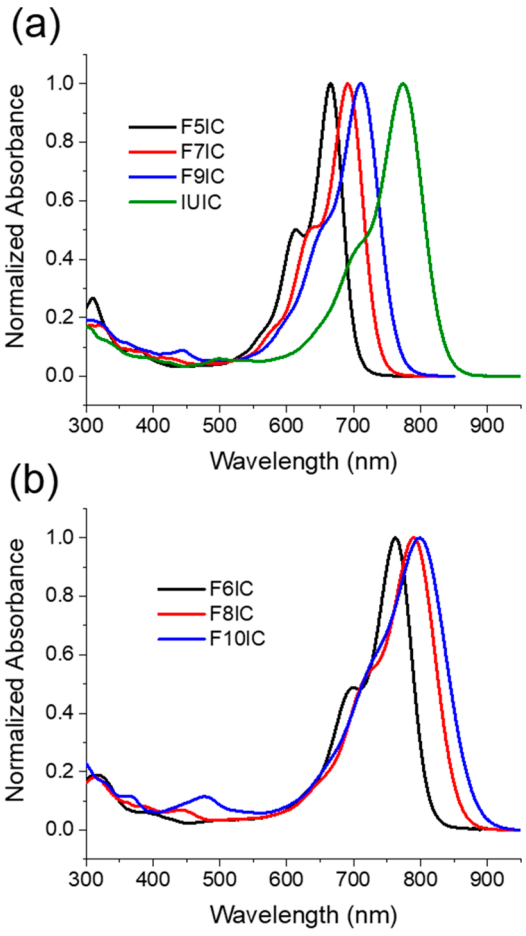

Figure 3. Normalized 1PA spectra in dilute chloroform solutions for the series of (a) indacene- and (b) TT-based cores.

F6IC, **F8IC**, and **F10IC** (Γ_{ge} = 159, 240, and 270 meV, respectively). Additional 1PA data such as the transition dipole moment (TDM) linking the ground state to the first excited-singlet state (M_{ge}) are summarized in Table 1. No evidence of aggregation was found, even at high concentrations (ca. 1−4 mM).

Nondegenerate Two-Photon Absorption. ND2PA spectra for indacene and TT compounds in ca. 1 mM chloroform solutions obtained via ND2PAS (λ_e = 1550 nm) are plotted in Figure 4a,b, respectively. OA Z-scan measurements (Figure 4c,d and Figures S1−S3) using wavelengths 1200 and 1300 nm were also performed for selected compounds in ca. 1.6−4.3 mM chloroform solutions and revealed ESA contributions consistent with longer-lived states seen by TA and high-fluence ND2PAS measurements, which will be discussed in detail later. In the present analysis, the maximum ND2PA cross-sections (δ_{max}, Table 1) from the predominantly instantaneous 2PA responses measured by ND2PAS at the lowest possible fluences will be examined comparatively for the purpose of identifying key structure−property relationships among indacene and TT compounds as a function of core size. The collective spectra in Figure 4a,b show that both sets of dyes demonstrated strong 2PA in the total transition wavelength range of 500−750 nm, which corresponded to a large range of degenerate wavelengths in the NIR (ca. 1000−1500 nm). Like 1PA spectra, 2PA bands shifted to longer wavelengths with an increasing number of rings, although the shifts were more significant relative to 1PA trends. In the indacene series for

https://dx.doi.org/10.1021/acs.jpca.0c02572
J. Phys. Chem. A XXXX, XXX, XXX−XXX

Table 1. Tabulated Values for Wavelengths at Maximum 1PA (λ_{max}^{1PA}), Molar Absorptivities (ε), 1PA Full Width at Half-Maximum (Γ_{ge}), g → e (M_{ge}) and e → e′ ($M_{ee'}$) TDMs, Wavelengths at Maximum 2PA (λ_{max}^{2PA}), and Maximum ND2PA Cross-Sections (δ_{max}) for the Indacene and TT Series

compound	λ_{max}^{1PA} (nm)[a]	ε (10^5 $M^{-1}cm^{-1}$)[a]	λ_{max}^{2PA} (nm)[c]	δ_{max} (10^3 GM)[c]	M_{ge} (D)[a,b]	$M_{ee'}$ (D)[d]	Γ_{ge} (meV)[a]
F5IC	665	1.89	1076	6.1	22.5	4.1	154
F7IC	691	2.10	1148	8.4	26.0	6.1	226
F9IC	710	2.17	1218	10	28.5	7.3	234
IUIC	774	2.76	1122	19	34.6		176
			1344	14		6.8	
F6IC	763	1.80[e]	1186	15	26.7	5.4	160
F8IC	790	2.10	1280	23	32.4	8.6	242
F10IC	799	2.00	1346	27	34.3	11	270

[a]In dilute (ca. 6−10 μM) chloroform solutions. [b]Calculated according to $M_{ge} = 0.09584 \times (\int \varepsilon \, d\nu/\nu_{max})^{0.5}$. [c]Obtained by ND2PAS (λ_e = 1550 nm) in ca. 1 μM chloroform solutions; error estimated to be ±15%. Wavelengths listed in terms of equivalent laser wavelengths. [d]Calculated according to eq 10. [e]Value reported in the literature.[33]

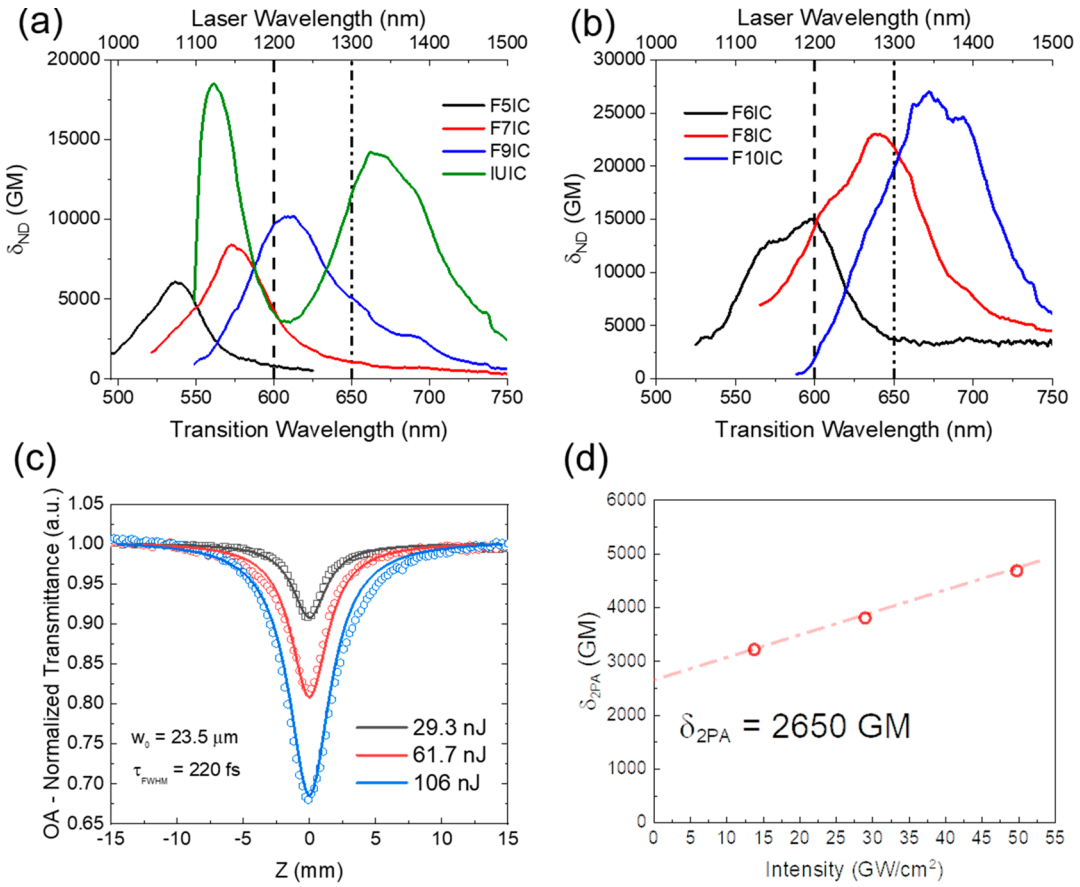

Figure 4. ND2PA spectra plotted in terms of ND2PA cross-sections vs transition wavelength and equivalent degenerate laser wavelength for ca. 1 mM chloroform solutions obtained by ND2PAS (λ_e = 1550 nm) of (a) indacene dyes and (b) TT dyes. (c) Examples of OA Z-scans and fits for **IUIC** in chloroform solution at 1200 nm using effective degenerate 2PA. (d) Plot of δ vs intensity showing intensity-dependent 2PA response for **IUIC** from Z-scan at 1200 nm. Vertical dashed and dash-dot lines on "a" and "b" show degenerate excitation wavelengths used for Z-scans at 1200 and 1300 nm, respectively.

example, shifts in terms of the equivalent laser wavelength for the transitions were 72 (**F5IC** to **F7IC**), 70 (**F7IC** to **F9IC**), and 126 nm (**F9IC** to **IUIC**). This trend was accompanied by an increase in δ_{max} with core size in both series (Table 1) with values varying from ca. 6−27 × 10^3 GM. The observed red-shifts indicate stabilization of the lowest-lying two-photon-allowed singlet state (presumed to be S_2)[46] with increasing numbers of rings and that the 2PA-allowed state is more stabilized in energy than S_1. As described by eq 1, enhancements in δ_{max} with increasing core size can be largely attributed to increases in the transition dipole moments (TDMs) from both $S_0 \rightarrow S_1$ (M_{ge}) and $S_1 \rightarrow S_2$ ($M_{ee'}$). M_{ge} for each compound was obtained via integration of the primary absorption band from 1PA spectra in dilute chloroform solutions (see comments in Table 1 for details), and $M_{ee'}$ values were estimated according to

$$M_{ee'} \approx \left(\frac{\Gamma_{ge}\delta_{max}}{KM_{ge}^2}\right)^{1/2}\left(\frac{1}{E_{ge} - \hbar\omega_1} + \frac{1}{E_{ge} - \hbar\omega_2}\right)^{-1} \quad (10)$$

https://dx.doi.org/10.1021/acs.jpca.0c02572
J. Phys. Chem. A XXXX, XXX, XXX−XXX

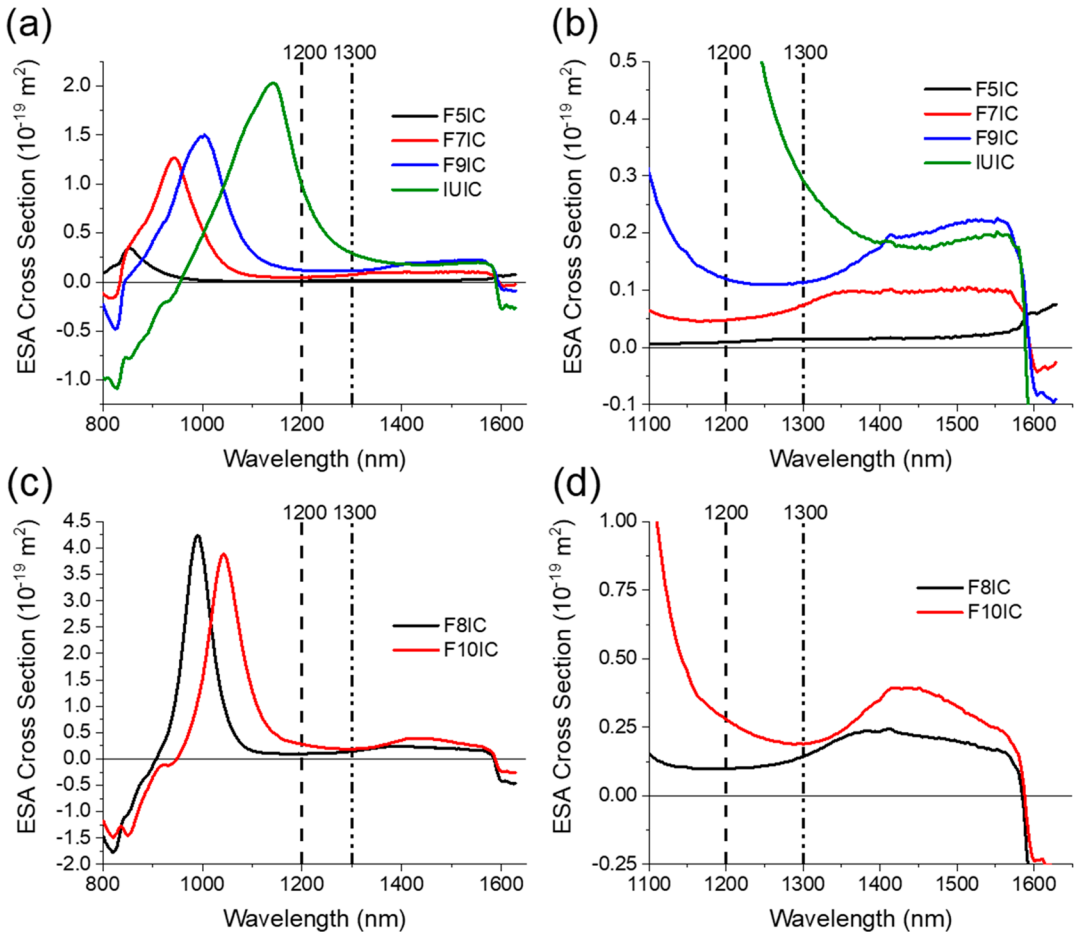

Figure 5. NIR, one-photon (λ_e= 720 nm) ESA spectra at ca. 100 fs temporal delay in ca. 0.1 mM chloroform solutions for (a) indacene dyes; (b) expanded indacene dye NIR ESA spectra showing the bands assigned to $S_1 \rightarrow S_3$ transitions between 1100 and 1600 nm; (c) TT dyes **F8IC** and **F10IC**; (d) expanded TT dye NIR ESA spectra showing bands assigned to $S_1 \rightarrow S_3$ between 1100 and 1600 nm. Vertical dashed and dash-dotted lines show degenerate excitation wavelengths used for Z-scans at 1200 and 1300 nm, respectively.

where K and other parameters were described earlier in the introduction of eqs 1 and 2. For all the materials in this study, $M_{ee'}$ values were calculated using Γ_{ge} obtained from the full width at half-maximum of the corresponding normalized 1PA spectrum, and frequencies ω_1 and ω_2 are assigned to the probe and pump beam, respectively.[7]

Examining the impact of TDMs on the observed 2PA trends, all compounds in these two series exhibited values of M_{ge} (ca. 22−34 D) that are large compared to those of well-studied quadrupolar compounds,[13,47−50] and large 2PA cross-sections that increased appreciably when more rings were added to the core. Due to the quadratic dependence of the 2PA response on M_{ge} (eq 1), the increase in M_{ge} with core size contributed significantly to the magnitudes of δ_{max} observed for both indacene and TT dyes. Although M_{ge} values for TT dyes (26.7−34.3 D) were comparable to similar-sized cores from the indacene series (26.0−34.6 D for **F7IC**, **F9IC**, and **IUIC**), in certain cases, TT compounds demonstrated slightly larger $M_{ee'}$ values than even some of their indacene counterparts with higher ring counts, i.e., **F8IC** (8.6 D) compared to **F9IC** and **IUIC** (7.3 and 6.8 D, respectively), and **F10IC** (11 D) compared to **F1IC** (6.8 D). Given modest differences in K, Γ_{ge}, and the detuning term $(1/E_{ge} - \hbar\omega_1 + 1/E_{ge} - \hbar\omega_2)$ between indacene- and TT-dyes of comparable core size (Table S4), the greater 2PA for the TT-series is likely mostly attributable to larger $M_{ee'}$ values. This result suggests that 2PA enhancement in TT-dyes is likely related to an increased coupling between the 1PA (S_1) and 2PA (S_2) active states that is facilitated by the presence of the dithienothiophene moiety in the center of the core.

These observations are consistent with previous studies of structurally similar dipolar and quadrupolar NLO molecules with dithienothiophene-containing, π-conjugated cores that demonstrated improved degenerate δ_{max} values relative to compounds with stilbene-, 9,10-dihydrophenanthrene-, and fluorene-based cores.[48,51,52] Furthermore, investigations involving thiophene-based π-linkers in dipolar and quadrupolar NLO chromophores have shown enhanced intramolecular charge transfer due to the presence of thiophene rings along the π-conjugated backbone for second- and third-order NLO applications.[53−56] The observed increase in 2PA for the TT compounds studied here might be describable in a similar way, although theoretical calculations would be necessary for confirmation. That is, the intramolecular charge transfer upon excitation was increased (potentially reflected in the trends of $M_{ee'}$ discussed previously) relative to that in the indacene dyes due to judicious substitution of exceptionally planar, electron-rich, fused-thiophene heterocycles in the center of the molecule that contributed significant π-electron density to a highly delocalized, π-conjugated chromophore.[48] Moreover, if TT compounds possessed strongly localized hole wave functions in the center of the molecule (i.e., center TT

https://dx.doi.org/10.1021/acs.jpca.0c02572
J. Phys. Chem. A XXXX, XXX, XXX−XXX

Table 2. Tabulated Values of D2PA Cross-Sections at Zero Irradiance ($\delta_{Z\text{-}\lambda}$) from OA Z-Scans and Values of ESA Cross-Sections (σ_λ) Obtained Using the TA Ground-State Depletion Method (GSD)[40] and by OA Z-Scans for the Indacene and TT Series (λ = 1200 and 1300 nm)

compound	$\delta_{Z\text{-}1200}$ (GM)[a]	σ_{1200} (10^{-19} m^2) GSD	σ_{1200} (10^{-19} m^2) Z-scan	$\delta_{Z\text{-}1300}$ (GM)[a]	σ_{1300} (10^{-19} m^2) GSD	σ_{1300} (10^{-19} m^2) Z-scan
F5IC	230	0.015	0.028		0.015	
F7IC	1000	0.049			0.077	
F9IC	7300	0.109		1000	0.105	0.085
IUIC	2700	1.000	0.031	2100	0.280	0.113
F6IC	2600					
F8IC		0.098		4900	0.143	0.030
F10IC		0.261		5300	0.182	0.019

[a]Estimated error is ±20%

rings) but still afforded substantial electron transfer toward the acceptors at the periphery of the molecule upon excitation, this could result in sizable enhancements to the quadrupolar polarization and further amplify the 2PA response for these types of compounds.[6,10,49]

Interestingly, **IUIC** showed two strong 2PA maxima (Figure 4a) in the measurable NIR window at a single pump wavelength (1550 nm), with one peak at the degenerate wavelength of 1344 nm (roughly consistent with extrapolation of the trends seen in **F5−9IC**) and a higher energy transition centered at 1122 nm. Given the small energy gap between these transition energies (ca. 370 meV) and the absence of any obvious 1PA transitions in the 1PA spectrum between $S_0 \rightarrow S_1$ and the transition energy of the higher energy 2PA band, the higher energy transition is likely attributable to $S_0 \rightarrow S_3$. The higher energy transition also shows a larger δ_{max} (19×10^3 GM) than $S_0 \rightarrow S_2$ (14×10^3 GM at 1344 nm). Reasonably, assuming the final S_3 state is also coupled to the intermediate S_1 state and that this transition is qualitatively described by a three-level model (eq 1), the greater δ_{max} for the 1122 nm band was attributed to a smaller detuning ($E_{ge} - \hbar\omega_1$) between the incident probe photon ($\hbar\omega_1$) and $S_0 \rightarrow S_1$ transition (E_{ge}), which resulted in greater resonance enhancement. Similar multiband 2PA spectra have been observed for quadrupolar polymethines, squaraines, and bis(acceptor)-terminated chromophores with bis(thiophene)vinylene π-bridges.[47,48,57] Due to the spectral range limitations of the spectrometer and the onset of 1PA bleach at ca. 800 nm for compounds with large cores, it was not possible to ascertain whether analogous bands were present for the other indacene and TT dyes.

Excited State Absorption Contributions to Two-Photon Absorption. OA Z-scan measurements (Figure 4c and Figures S1−S3) in chloroform solutions showed irradiance-dependent D2PA cross-sections for some compounds, which indicates an ESA contribution to the 2PA response; presumably this arises from rapid $S_2 \rightarrow S_1$ relaxation and subsequent absorption to a higher-lying singlet state on the back end of the excitation pulse. The presence of appreciable ESA at excitation wavelengths used for Z-scan (λ = 1200 and 1300 nm) was confirmed with TA measurements for all compounds by acquiring spectra over ca. 1 ps time delays following one- ($S_0 \rightarrow S_1$) and two-photon excitation ($S_0 \rightarrow S_2$). NIR ESA spectra for indacene (Figure 5a,b) and TT compounds (Figure 5c,d) showed two bands, the strongest of which was likely a higher-energy $S_1 \rightarrow S_n$ transition[58] and the less intense, broader transition at longer wavelengths was ascribed to $S_1 \rightarrow S_3$ ($|e\rangle \rightarrow |e''\rangle$); see Figure S4a,b for Jabłoński diagrams and Figure 5b,d for expanded plots of the $S_1 \rightarrow S_3$ bands. In comparing the bandwidths of each core type, the higher energy bands for indacene compounds (FWHM = 116−151 meV) were considerably broader than TT dyes **F8IC** and **F10IC** (FWHM = 82 and 86 meV, respectively). Furthermore, the $S_1 \rightarrow S_3$ peaks were still broad but more well-defined for TT dyes which, along with the substantially narrower $S_1 \rightarrow S_n$ bands, could possibly be explained by TT compounds exhibiting less conformational heterogeneity in these states compared to their indacene counterparts.[25] Additional TA measurements were performed with a visible broadband probe to identify higher-lying excited states that did not contribute to 2PA. These ESA spectra (Figure S5), were used to determine maximum ESA cross-sections of all observable transitions (Table S1).

To investigate the origin of the effective 2PA response in OA Z-scan, the spectral overlap of 2PA and NIR ESA bands were analyzed for both series of cores. Like 1PA and 2PA spectra, local ESA maxima generally red-shifted with increasing core size (Figure 5 and Figure S4). The λ_{max}^{2PA} and majority of the 2PA bandwidth for **F5IC**, **F7IC**, and **F9IC** were located between the two ESA bands (Figure S6a−c) of each compound, which precluded the unambiguous determination of specific excited-state contributions to effective 2PA. However, this trend did not extend to **IUIC** from the indacene series for which considerable overlap between the $S_1 \rightarrow S_n$ band and both 2PA bands was observed (Figure S6d). The reasons for such deviation were 3-fold: **IUIC** demonstrated (1) relatively moderate differences between λ_{max}^{2PA} and λ_{max}^{ESA} for the $S_1 \rightarrow S_n$ transition (shift = 204 nm), (2) a larger FWHM (i.e., 211 meV) for the λ_{max}^{2PA} = 1344 nm transition, and (3) a significantly red-shifted $S_1 \rightarrow S_3$ band, the peak for which likely appeared outside the measurable range (>1600 nm). It is noted that the estimated peak position of $S_1 \rightarrow S_3$ (ca. 2040 nm) is consistent with the λ_{max}^{2PA} for the $S_0 \rightarrow S_3$ 2PA transition measured via ND2PAS. Compared to the 2PA-ESA peak shifts of their indacene counterparts (204−223 nm for **F5-IUIC**, Table S3) with increasing core size, **F8IC** and **F10IC** showed greater shifts (290 and 306 nm, respectively) and smaller $S_1 \rightarrow S_n$ ESA fwhm (Table S1) that counteracted the larger 2PA FWHM values and resulted in little-to-no 2PA overlap with the $S_1 \rightarrow S_n$ bands. Moreover, because the $S_1 \rightarrow S_3$ peaks for TT compounds were slightly blue-shifted (Figure 5d) compared to similar sized indacene cores (i.e., **F9,IUIC**, Figure 5b), substantial 2PA overlap with this transition was observed (Figure S7) and thus the $S_1 \rightarrow S_3$ transition was presumed to be the largest ESA contributor to effective 2PA for TT dyes near λ_{max}^{2PA}. D2PA cross-sections extrapolated to zero irradiance ($\delta_{Z\text{-}\lambda}$) at λ = 1200 and 1300 nm obtained by OA Z-scan and corresponding ESA cross-sections (σ_λ) are listed in Tables 2 and S2. Because most samples were not pumped directly at

https://dx.doi.org/10.1021/acs.jpca.0c02572
J. Phys. Chem. A XXXX, XXX, XXX−XXX

λ_{max}^{2PA}, the distribution in observed $\delta_{Z\text{-}\lambda}$ and σ_λ values were naturally complicated by how efficiently two-photon excited states (S_2) were generated and the subsequent S_1 population available for ESA over the duration of the pulse. Compared to ESA cross-sections at λ = 1200 and 1300 nm obtained using the ground-state depletion method[40] (Table S2), values of σ_λ extracted from Z-scan were similar in magnitude, typically on the order of 10^{-21} m^2, but did not match quantitatively, likely for reasons described above. Taking **IUIC** for example, one might expect σ_{1200} to be larger than σ_{1300} because of the inherently larger ESA cross-section measured by TA at 1200 nm (Figure 5a,b and Table S2). However, the larger value of σ_{1300} obtained via Z-scan (relative to σ_{1200} from Z-scan) and disparity between values of σ_{1200} obtained by TA and Z-scan for **IUIC** were likely explained by significantly larger 2PA efficiency at 1300 nm (Figure 5a) compared to 1200 nm that resulted in a greater excited-state population and thus a larger slope due to increased ESA. In terms of the overall ESA contribution to the effective 2PA response, the relatively small magnitudes of σ_λ (ca. 10^{-21} m^2) near λ_{max}^{2PA} for most compounds confirmed by Z-scan and TA indicated that the ESA component was appreciable, but the response was predominantly instantaneous 2PA, as was suspected from ND2PA measurements. These findings were reasonable given that one would not expect a large buildup of excited states over the ca. 100 fs pulse widths used in this investigation. Regarding the D2PA cross-sections at zero irradiance reported here, a comparison of their magnitudes relative to the nondegenerate cross-sections discussed so far is beyond the scope of this investigation and otherwise unreliable without further experiments due to the indirect relation between the two.[7] Moreover, although the largest D2PA cross-sections here (7300 GM for **F7IC** at 1200 nm; 5300 GM for **F10IC** at 1300 nm) are of comparable magnitude to the largest cross-sections reported for a variety of organic and metal-chromophores at similar wavelengths,[6,22,23,25,27] these comparisons should be made with caution, due to the irradiance dependence and necessity for extrapolation to zero-irradiance for the present compounds.

Influence of End Groups on One- and Two-Photon Absorption. *One-Photon Absorption.* Normalized 1PA spectra in dilute chloroform solutions (ca. 1−10 μM) for seven-ring, indacene-based compounds **ITIC**, **ITIC3**, **F7IC**, and **ITBC** are plotted in Figure 6. The reported reduction potentials for films of these compounds shift to increasingly reducing (more negative) potential in the order **ITIC**[31] < **ITIC3**[34] < **F7IC**[33] < **ITBC**,[39] suggesting that the acceptor strength of the end groups increases in the same order. Previous studies of quadrupolar A-D-A chromophores[10,48] show bathochromic shifts of the 1PA band with increasing acceptor strength; the successively bathochromically shifted 1PA and concomitantly increased M_{ge} values in the present series, as summarized in Table 3, is consistent with this behavior and with the acceptor strength implied by the reduction potentials. Although the longest wavelength absorbing dye (**ITBC**) demonstrated a λ_{max}^{1PA} (719 nm) slightly longer than that of **F9IC** (710 nm), it was still considerably shorter than that of **IUIC** (774 nm). In addition to smaller spectral shifts with the range of acceptors examined here compared to those observed as a function of ring count for **F5-IUIC**, these results revealed that changes in indacene core size were more effective in extending 1PA further into the NIR. Even at high concentrations (ca. 1−4 mM), no evidence of aggregation was found.

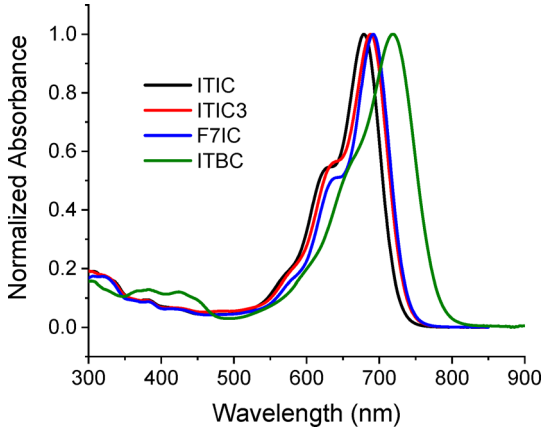

Figure 6. Normalized absorption spectra for **ITIC**, **ITIC3**, **F7IC**, and **ITBC** in dilute (ca. 1−10 μM) chloroform solutions.

Nondegenerate Two-Photon Absorption. ND2PA spectra in ca. 1 mM chloroform solutions for the varied-acceptor series are shown in Figure 7a. Like their 1PA spectra, λ_{max}^{2PA} red-shifted with increasing acceptor strength (Table 3), although not to the extent of indacene and TT dyes. This trend was mirrored by the values obtained for δ_{max} which, when considering experimental error (ca. ±15%), did not demonstrate significant 2PA enhancement. In addition to small 1PA and 2PA spectral shifts, smaller magnitudes of M_{ge} (24.8−26.4 D) and $M_{ee'}$ (6.1−6.7 D) relative to indacene and TT dyes with larger cores (Table 1) suggested that increasing acceptor strength (within the range examined here) did not amplify quadrupolar charge transfer as effectively as core-structure modifications. Moreover, the shorter λ_{max}^{1PA} (i.e., larger E_{ge} values) for this series limited the degree to which these compounds benefited from resonance enhancement. However, efforts to tune 2PA for A-π-D-π-A molecules via changes in end group functionalities should not be disregarded, as the application of such strategies to promising dyes such as **F8IC** and **F10IC** could afford greater resonance enhancements via substantially red-shifted 1PA that could further benefit 2PA in the NIR. Additionally, judicious substitution with stronger acceptors than those studied here presents opportunities to achieve sizable NIR 1PA and/or 2PA with smaller chromophores that potentially affords reduced synthetic complexity, improved flexibility, and the ability to obtain lower molecular weight chromophores that are desirable for applications requiring high number density films, such as optical limiting.

Excited-State Absorption Contributions to Two-Photon Absorption. Regarding the possible role of ESA in 2PA for the varied-acceptor series, NIR ESA spectra in Figure 7b,c and 2PA-ESA overlaid spectra in Figures S6b and S8 show λ_{max}^{2PA} overlap in the region of intersecting tails between the bands assigned to $S_1 \rightarrow S_3$ and $S_1 \rightarrow S_n$ bands. As such, the dominant ESA contributor could not be unambiguously identified; as in the case of **F5IC**, **F7IC**, and **F9IC** from the indacene series, this is due to comparable shifts between ESA and 2PA bands as a function of acceptor strength that resulted in poor spectral overlap with either of the nearby ESA transitions in this spectral window (Table S3). Only OA Z-scans at λ = 1200 nm (Table 4) from **ITIC** and **ITIC3** in this series demonstrated considerable irradiance-dependent 2PA slopes (Figure S9a−d) from which σ_{1200} could be estimated and gave ESA cross-sections (ca. 2.8 × 10^{-21} m^2) that agreed reasonably well with

https://dx.doi.org/10.1021/acs.jpca.0c02572
J. Phys. Chem. A XXXX, XXX, XXX−XXX

Table 3. Tabulated Values for Wavelengths at Maximum 1PA (λ_{max}^{1PA}), Molar Absorptivities (ε), 1PA Full Width at Half Maximum (Γ_{ge}), g → e (M_{ge}) and e → e′ ($M_{ee'}$) TDMs, Wavelengths at Maximum 2PA (λ_{max}^{2PA}), and Maximum ND2PA Cross-Sections (δ_{max}) for the Varied-Acceptor Series

compound	λ_{max}^{1PA} (nm)[a]	ε (10^5 $M^{-1}cm^{-1}$)[a]	λ_{max}^{2PA} (nm)[c]	δ_{max} (10^3 GM)[c]	M_{ge} (D)[a,b]	$M_{ee'}$ (D)[d]	Γ_{ge} (meV)[a]
ITIC	679	1.92	1130	7.3	24.8	6.2	251
ITIC3	688	1.94	1142	7.5	25.6	6.1	253
F7IC	691	2.10	1148	8.4	26.0	6.1	226
ITBC	719	1.65	1192	8.6	26.4	6.7	258

[a]In dilute (ca. 1−10 μM) chloroform solutions. [b]Calculated according to $M_{ge} = 0.09584 \times (\int \varepsilon \, d\nu/\nu_{max})^{0.5}$. [c]Obtained by ND2PAS (λ_e = 1550 nm) in ca. 1 μM chloroform solutions; error estimated to be ±15%. Wavelengths listed in terms of equivalent degenerate laser wavelengths. [d]Calculated according to eq 10.

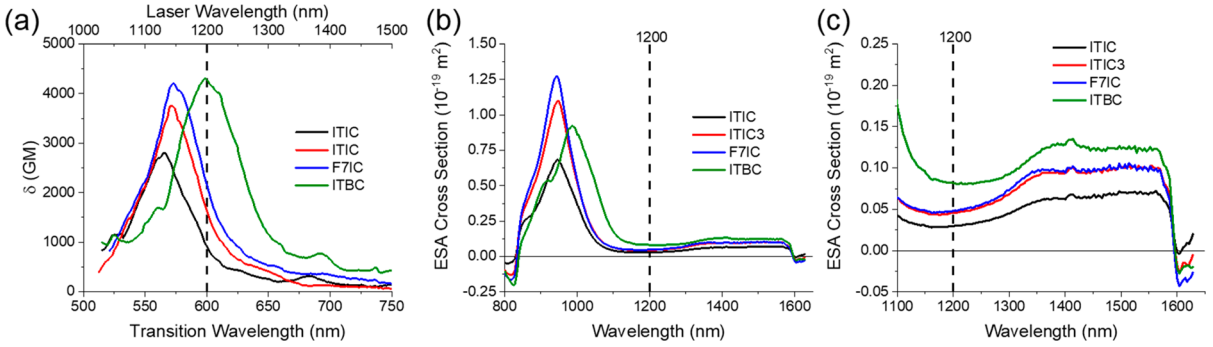

Figure 7. For the series **ITIC**, **ITIC3**, **F7IC**, and **ITBC**: (a) 2PA spectra plotted in terms of ND2PA cross-sections vs transition wavelength and equivalent degenerate laser wavelength for ca. 1 mM chloroform solutions obtained by ND2PAS (λ_e = 1550 nm), (b) NIR ESA spectra (λ_e = 720 nm) at ca. 100 fs delay in ca. 0.1 mM chloroform solutions, and (c) expanded NIR ESA spectra showing the $S_1 \rightarrow S_3$ bands between 1100 and 1600 nm. Vertical dashed lines show the degenerate excitation wavelength used for OA Z-scans at 1200 nm.

Table 4. Tabulated Values of D2PA Cross-Sections at Zero Irradiance ($\delta_{Z\text{-}\lambda}$) from OA Z-Scans and Values of ESA Cross-Sections (σ_λ) Obtained Using the TA Ground-State Depletion (GSD) Method[40] and by OA Z-Scans for ITIC, ITIC3, F7IC, and ITBC

compound	$\delta_{Z\text{-}1200}$ (GM)[a]	σ_{1200} (10^{-19} m^2) GSD	σ_{1200} (10^{-19} m^2) Z-scan
ITIC	810	0.032	0.028
ITIC3	600	0.049	0.029
F7IC	1100	0.049	
ITBC	3800	0.081	

[a]Estimated error ±20%

those obtained via TA measurements (Tables 4 and S2). However, the reason for this is unclear given that ESA for the other compounds in this series was comparable or stronger at 1200 nm (Figure 7c) and λ_{max}^{2PA} for these compounds were closer to resonance with 1200 nm, albeit slightly in the case of **F7IC**, than **ITIC** and **ITIC3**. Additionally, it was noted that the progression of σ_{S1-Sn} ($S_1 \rightarrow S_n$ band) with acceptor strength (Table 3) mirrored 1PA (ε) trends but the continual increase in intensity of the $S_1 \rightarrow S_3$ band did not. This was unlike what was seen in the **F5IC**, **F7IC**, **F9IC**, and **IUIC** series where, generally, both bands intensified upon the addition of more rings.

CONCLUSIONS

The influence of core size and acceptor strength on the 1PA and 2PA spectral shifts and the 2PA responses for a series of highly conjugated, fused-ring, quadrupolar type A-π-D-π-A chromophores have been examined. ND2PA measurements revealed that increasing core size (i.e., π-conjugation length) and acceptor strength resulted in greater π-electron delocalization that bathochromically shifted 2PA bands (Figure 4a,b and Figure 7a) further into the NIR thereby covering an impressive spectral range (ca. 1000−1500 nm). Furthermore, compounds with larger cores generally showed enhanced ND2PA, which resulted in larger δ_{max} values. 2PA enhancement for these materials was largely attributed to amplified charge transfer upon excitation (i.e., increasing TDM values, M_{ge} and $M_{ee'}$) for dyes with more fused rings. As such, TT dyes demonstrated considerably larger 2PA than their indacene counterparts, which was presumably due to the presence of π-electron-rich thiophene heterocycles in the place of phenyl moieties that shifted λ_{max}^{1PA} and λ_{max}^{2PA} to considerably longer wavelengths and showed some of the largest M_{ge} and $M_{ee'}$ values among all compounds in this work. Notably, **F10IC** and **IUIC** demonstrated large 2PA (ca. λ_{max}^{2PA} = 1350 nm) in the short-wavelength part of the telecommunications window (1300−1600 nm).

The origin of ESA contributions to the effective 2PA response measured by OA Z-scan was investigated by TA and showed that λ_{max}^{2PA} for most compounds overlapped with a region of intersecting NIR band tails ascribed to the $S_1 \rightarrow S_3$ and $S_1 \rightarrow S_n$ transitions. As a result, the exact transition giving rise to effective 2PA could not be clearly identified. However, both 2PA bands from **IUIC** showed sizable overlap with its $S_1 \rightarrow S_n$ transition and those for **F8IC** and **F10IC** overlapped appreciably with their respective $S_1 \rightarrow S_3$ transitions, from which the ESA contributions were presumed. Although ESA was found to be appreciable near 2PA resonances for most compounds, the generally smaller ESA cross-sections (ca. 10^{-21} m^2) near λ_{max}^{2PA} and short pulse widths (ca. 100 fs) are typically not conducive to obtaining large excited-state populations and suggest that the effective response was predominantly

https://dx.doi.org/10.1021/acs.jpca.0c02572
J. Phys. Chem. A XXXX, XXX, XXX−XXX

instantaneous 2PA. Interestingly, ESA cross-sections (σ_{S1-Sn}) at the transition maximum assigned to ($S_1 \rightarrow S_n$) for some indacene compounds were ca. 1.5−1.9 times greater than their ground-state absorption cross-sections (σ_{GS}, TableS1) and those for TT dyes **F8IC** and **F10IC** were ca. 5 times larger, potentially making these compounds attractive reverse saturable absorbers for NIR optical limiting.

Compared to well-known quadrupolar bis(styryl)benzenes, oligophenylenevinylenes, polymethines, and squaraines, the 2PA bands for the fused-ring compounds studied here absorbed at comparable or even slightly longer wavelengths (ca. 1100−1500 nm).[10,13,17,18,47,49,59] Additionally, ND2PA δ_{max} values demonstrated by the entire TT-series and **IUIC** (14−27 × 10^3 GM) were larger than values reported for thoroughly studied D-A-D fluorene[7] molecules and A-π-D-π-A compounds with bis(heterocycle)vinylene bridges,[48] and comparable to those for highly π-conjugated squaraine dyes[17] and diphenylaminofluorene-based[60] oligomers and polymers (ca. 15−20 × 10^3 GM).

It is remarkable that ND2PA for these discrete molecular systems was competitive with and, in some cases, greater than that for oligomeric/polymeric compounds. Such a result highlights the promising 2PA performance that can be obtained with A-π-D-π-A compounds by exploiting the wealth of chemistries available to judiciously tune their structure and thus optoelectronic properties. In summary, this investigation presented a significant advance in understanding key structure−property relationships that controlled 2PA and ESA for novel fused-ring compounds that could inform the design of future generations of 2PA materials.

■ ASSOCIATED CONTENT

Supporting Information

The Supporting Information is available free of charge at https://pubs.acs.org/doi/10.1021/acs.jpca.0c02572.

Additional Z-scan graphs and data, additional ESA spectra, photophysical energy diagrams and charts, additional tabulated optical data and values used in calculations of δ_{max} (PDF)

■ AUTHOR INFORMATION

Corresponding Authors

Seth R. Marder − *School of Chemistry and Biochemistry, Center for Organic Photonics, Georgia Institute of Technology, Atlanta, Georgia 30332-0400, United States;* orcid.org/0000-0001-6921-2536; Email: seth.marder@chemistry.gatech.edu

Joseph W. Perry − *School of Chemistry and Biochemistry, Center for Organic Photonics, Georgia Institute of Technology, Atlanta, Georgia 30332-0400, United States;* Email: joe.perry@gatech.edu

Authors

Taylor G. Allen − *School of Chemistry and Biochemistry, Center for Organic Photonics, Georgia Institute of Technology, Atlanta, Georgia 30332-0400, United States;* orcid.org/0000-0003-0829-4165

Sepehr Benis − *CREOL, The College of Optics & Photonics, University of Central Florida, Orlando, Florida 32816-2700, United States;* orcid.org/0000-0002-5442-7021

Natalia Munera − *CREOL, The College of Optics & Photonics, University of Central Florida, Orlando, Florida 32816-2700, United States*

Junxiang Zhang − *School of Chemistry and Biochemistry, Center for Organic Photonics, Georgia Institute of Technology, Atlanta, Georgia 30332-0400, United States*

Shuixing Dai − *Department of Materials Science and Engineering, College of Engineering, Peking University, Beijing 100871, People's Republic of China*

Tengfei Li − *Department of Materials Science and Engineering, College of Engineering, Peking University, Beijing 100871, People's Republic of China*

Boyu Jia − *Department of Materials Science and Engineering, College of Engineering, Peking University, Beijing 100871, People's Republic of China*

Wei Wang − *Department of Materials Science and Engineering, College of Engineering, Peking University, Beijing 100871, People's Republic of China*

Stephen Barlow − *School of Chemistry and Biochemistry, Center for Organic Photonics, Georgia Institute of Technology, Atlanta, Georgia 30332-0400, United States;* orcid.org/0000-0001-9059-9974

David J. Hagan − *CREOL, The College of Optics & Photonics, University of Central Florida, Orlando, Florida 32816-2700, United States;* orcid.org/0000-0003-2713-1767

Eric W. Van Stryland − *CREOL, The College of Optics & Photonics, University of Central Florida, Orlando, Florida 32816-2700, United States*

Xiaowei Zhan − *Department of Materials Science and Engineering, College of Engineering, Peking University, Beijing 100871, People's Republic of China;* orcid.org/0000-0002-1006-3342

Complete contact information is available at: https://pubs.acs.org/10.1021/acs.jpca.0c02572

Author Contributions

S.R.M. and T.G.A. conceived of the project. T.G.A. conducted linear and ND2PAS characterization and analyses and wrote the manuscript. S. Benis and N.M. performed OA Z-scans, assisted with calculations, and contributed to the manuscript. J.Z. synthesized varied-acceptor compounds. S.D., T.L., B.J., and W.W. synthesized varied-core compounds. S. Barlow, D.J.H., E.W.V.S., X.Z., J.W.P., and S.R.M. are the senior investigators for their respective groups. The manuscript was written through contributions of all authors. All authors have given approval to the final version of the manuscript.

Notes

The authors declare no competing financial interest.

■ ACKNOWLEDGMENTS

This work was funded in part by the Office of Naval Research (N00014-17-1-2243). S. Benis, N.M., D.J.H., and E.W.V.S. thank the Army Research Lab (W911NF-15-2-0090) for support. N.M. also thanks the UCF Pre-eminent Postdoctoral Program for funding. T.G.A. thanks San-Hui Chi and Joel Hales for helpful discussions regarding ND2PA measurements.

■ ABBREVIATIONS

1PA, one-photon absorption; 2PA, two-photon absorption; ESA, excited-state absorption; TT, thieno[3,2-*b*]thiophene; TA, transient absorption; D2PA, degenerate two-photon absorption; ND2PA, nondegenerate two-photon absorption; TDM, transition dipole moment; FWHM, full width at half-maximum; GSD, ground-state depletion

https://dx.doi.org/10.1021/acs.jpca.0c02572
J. Phys. Chem. A XXXX, XXX, XXX−XXX

REFERENCES

(1) Stirman, J. N.; Smith, I. T.; Kudenov, M. W.; Smith, S. L. Wide Field-of-View, Multi-Region, Two-Photon Imaging of Neuronal Activity in the Mammalian Brain. *Nat. Biotechnol.* **2016**, *34*, 857.

(2) Yee, D. W.; Schulz, M. D.; Grubbs, R. H.; Greer, J. R. Functionalized 3D Architected Materials Via Thiol-Michael Addition and Two-Photon Lithography. *Adv. Mater.* **2017**, *29*, 1605293.

(3) Price, R. S.; Dubinina, G.; Wicks, G.; Drobizhev, M.; Rebane, A.; Schanze, K. S. Polymer Monoliths Containing Two-Photon Absorbing Phenylenevinylene Platinum(II) Acetylide Chromophores for Optical Power Limiting. *ACS Appl. Mater. Interfaces* **2015**, *7*, 10795−10805.

(4) Dvornikov, A. S.; Walker, E. P.; Rentzepis, P. M. Two-Photon Three-Dimensional Optical Storage Memory. *J. Phys. Chem. A* **2009**, *113*, 13633−13644.

(5) Terenziani, F.; Katan, C.; Badaeva, E.; Tretiak, S.; Blanchard-Desce, M. Enhanced Two-Photon Absorption of Organic Chromophores: Theoretical and Experimental Assessments. *Adv. Mater.* **2008**, *20*, 4641−4678.

(6) Pawlicki, M.; Collins, H. A.; Denning, R. G.; Anderson, H. L. Two-Photon Absorption and the Design of Two-Photon Dyes. *Angew. Chem., Int. Ed.* **2009**, *48*, 3244−3266.

(7) Hales, J. M.; Hagan, D. J.; Van Stryland, E. W.; Schafer, K. J.; Morales, A. R.; Belfield, K. D.; Pacher, P.; Kwon, O.; Zojer, E.; Bredas, J. L. Resonant Enhancement of Two-Photon Absorption in Substituted Fluorene Molecules. *J. Chem. Phys.* **2004**, *121*, 3152−3160.

(8) Ensley, T. R.; Hu, H.; Reichert, M.; Ferdinandus, M. R.; Peceli, D.; Hales, J. M.; Perry, J. W.; Li, Z. a.; Jang, S.-H.; Jen, A. K. Y.; et al. Quasi-Three-Level Model Applied to Measured Spectra of Nonlinear Absorption and Refraction in Organic Molecules. *J. Opt. Soc. Am. B* **2016**, *33*, 780−796.

(9) The vacuum permittivity variable in the denominator of *K* in ref 7 should be squared. The correct equation is displayed in eq 2 and was checked against ref 8 for validity.

(10) Albota, M.; Beljonne, D.; Brédas, J.-L.; Ehrlich, J. E.; Fu, J.-Y.; Heikal, A. A.; Hess, S. E.; Kogej, T.; Levin, M. D.; Marder, S. R.; et al. Design of Organic Molecules with Large Two-Photon Absorption Cross Sections. *Science* **1998**, *281*, 1653−1656.

(11) Scherer, D.; Dörfler, R.; Feldner, A.; Vogtmann, T.; Schwoerer, M.; Lawrentz, U.; Grahn, W.; Lambert, C. Two-Photon States in Squaraine Monomers and Oligomers. *Chem. Phys.* **2002**, *279*, 179−207.

(12) Beverina, L.; Crippa, M.; Salice, P.; Ruffo, R.; Ferrante, C.; Fortunati, I.; Signorini, R.; Mari, C. M.; Bozio, R.; Facchetti, A.; et al. Indolic Squaraines as Two-Photon Absorbing Dyes in the Visible Region: X-Ray Structure, Electrochemical, and Nonlinear Optical Characterization. *Chem. Mater.* **2008**, *20*, 3242−3244.

(13) Pond, S. J. K.; Rumi, M.; Levin, M. D.; Parker, T. C.; Beljonne, D.; Day, M. W.; Brédas, J.-L.; Marder, S. R.; Perry, J. W. One- and Two-Photon Spectroscopy of Donor−Acceptor−Donor Distyrylbenzene Derivatives: Effect of Cyano Substitution and Distortion from Planarity. *J. Phys. Chem. A* **2002**, *106*, 11470−11480.

(14) Forli, A.; Vecchia, D.; Binini, N.; Succol, F.; Bovetti, S.; Moretti, C.; Nespoli, F.; Mahn, M.; Baker, C. A.; Bolton, M. M.; et al. Two-Photon Bidirectional Control and Imaging of Neuronal Excitability with High Spatial Resolution in Vivo. *Cell Rep.* **2018**, *22*, 3087−3098.

(15) Zheng, W.; Huang, P.; Gong, Z.; Tu, D.; Xu, J.; Zou, Q.; Li, R.; You, W.; Bünzli, J.-C. G.; Chen, X. Near-Infrared-Triggered Photon Upconversion Tuning in All-Inorganic Cesium Lead Halide Perovskite Quantum Dots. *Nat. Commun.* **2018**, *9*, 3462.

(16) Li, D.; Jing, P.; Sun, L.; An, Y.; Shan, X.; Lu, X.; Zhou, D.; Han, D.; Shen, D.; Zhai, Y.; et al. Near-Infrared Excitation/Emission and Multiphoton-Induced Fluorescence of Carbon Dots. *Adv. Mater.* **2018**, *30*, 1705913.

(17) Chung, S.-J.; Zheng, S.; Odani, T.; Beverina, L.; Fu, J.; Padilha, L. A.; Biesso, A.; Hales, J. M.; Zhan, X.; Schmidt, K.; et al. Extended Squaraine Dyes with Large Two-Photon Absorption Cross-Sections. *J. Am. Chem. Soc.* **2006**, *128*, 14444−14445.

(18) Odom, S. A.; Webster, S.; Padilha, L. A.; Peceli, D.; Hu, H.; Nootz, G.; Chung, S.-J.; Ohira, S.; Matichak, J. D.; Przhonska, O. V.; et al. Synthesis and Two-Photon Spectrum of a Bis(Porphyrin)-Substituted Squaraine. *J. Am. Chem. Soc.* **2009**, *131*, 7510−7511.

(19) Mongin, O.; Porrès, L.; Charlot, M.; Katan, C.; Blanchard-Desce, M. Synthesis, Fluorescence, and Two-Photon Absorption of a Series of Elongated Rodlike and Banana-Shaped Quadrupolar Fluorophores: A Comprehensive Study of Structure−Property Relationships. *Chem. - Eur. J.* **2007**, *13*, 1481−1498.

(20) Lee, S. K.; Yang, W. J.; Choi, J. J.; Kim, C. H.; Jeon, S.-J.; Cho, B. R. 2,6-Bis[4-(*p*-dihexylaminostyryl)styryl]anthracene Derivatives with Large Two-Photon Cross Sections. *Org. Lett.* **2005**, *7*, 323−326.

(21) Beverina, L.; Fu, J.; Leclercq, A.; Zojer, E.; Pacher, P.; Barlow, S.; Van Stryland, E. W.; Hagan, D. J.; Brédas, J.-L.; Marder, S. R. Strong Two-Photon Absorption at Telecommunications Wavelengths in a Dipolar Chromophore with a Pyrrole Auxiliary Donor and Thiazole Auxiliary Acceptor. *J. Am. Chem. Soc.* **2005**, *127*, 7282−7283.

(22) Cho, J.-Y.; Barlow, S.; Marder, S. R.; Fu, J.; Padilha, L. A.; Van Stryland, E. W.; Hagan, D. J.; Bishop, M. Strong Two-Photon Absorption at Telecommunications Wavelengths in Nickel Bis-(Dithiolene) Complexes. *Opt. Lett.* **2007**, *32*, 671.

(23) Thorley, K. J.; Hales, J. M.; Anderson, H. L.; Perry, J. W. Porphyrin Dimer Carbocations with Strong near Infrared Absorption and Third-Order Optical Nonlinearity. *Angew. Chem., Int. Ed.* **2008**, *47*, 7095−7098.

(24) Drobizhev, M.; Stepanenko, Y.; Dzenis, Y.; Karotki, A.; Rebane, A.; Taylor, P. N.; Anderson, H. L. Extremely Strong near-Ir Two-Photon Absorption in Conjugated Porphyrin Dimers: Quantitative Description with Three-Essential-States Model. *J. Phys. Chem. B* **2005**, *109*, 7223−7236.

(25) Hales, J. M.; Cozzuol, M.; Screen, T. E. O.; Anderson, H. L.; Perry, J. W. Metalloporphyrin Polymer with Temporally Agile, Broadband Nonlinear Absorption for Optical Limiting in the near Infrared. *Opt. Express* **2009**, *17*, 18478−18488.

(26) Drobizhev, M.; Makarov, N. S.; Rebane, A.; de la Torre, G.; Torres, T. Strong Two-Photon Absorption in Push−Pull Phthalocyanines: Role of Resonance Enhancement and Permanent Dipole Moment Change Upon Excitation. *J. Phys. Chem. C* **2008**, *112*, 848−859.

(27) Pascal, S.; Bellier, Q.; David, S.; Bouit, P.-A.; Chi, S.-H.; Makarov, N. S.; Le Guennic, B.; Chibani, S.; Berginc, G.; Feneyrou, P.; et al. Unraveling the Two-Photon and Excited-State Absorptions of Aza-Bodipy Dyes for Optical Power Limiting in the SWIR Band. *J. Phys. Chem. C* **2019**, *123*, 23661−23673.

(28) Jia, J.; Zhang, Y.; Zheng, M.; Shan, C.; Yan, H.; Wu, W.; Gao, X.; Cheng, B.; Liu, W.; Tang, Y. Functionalized Eu(III)-Based Nanoscale Metal−Organic Framework to Achieve near-Ir-Triggered and -Targeted Two-Photon Absorption Photodynamic Therapy. *Inorg. Chem.* **2018**, *57*, 300−310.

(29) Wawrzynczyk, D.; Nyk, M.; Samoc, M. Multiphoton Absorption in Europium(III) Doped YVO_4 Nanoparticles. *J. Mater. Chem. C* **2013**, *1*, 5837−5842.

(30) Wenseleers, W.; Stellacci, F.; Meyer-Friedrichsen, T.; Mangel, T.; Bauer, C. A.; Pond, S. J. K.; Marder, S. R.; Perry, J. W. Five Orders-of-Magnitude Enhancement of Two-Photon Absorption for Dyes on Silver Nanoparticle Fractal Clusters. *J. Phys. Chem. B* **2002**, *106*, 6853−6863.

(31) Lin, Y.; Wang, J.; Zhang, Z.-G.; Bai, H.; Li, Y.; Zhu, D.; Zhan, X. An Electron Acceptor Challenging Fullerenes for Efficient Polymer Solar Cells. *Adv. Mater.* **2015**, *27*, 1170−1174.

(32) Dai, S.; Xiao, Y.; Xue, P.; James Rech, J.; Liu, K.; Li, Z.; Lu, X.; You, W.; Zhan, X. Effect of Core Size on Performance of Fused-Ring Electron Acceptors. *Chem. Mater.* **2018**, *30*, 5390−5396.

(33) Dai, S.; Li, T.; Wang, W.; Xiao, Y.; Lau, T.-K.; Li, Z.; Liu, K.; Lu, X.; Zhan, X. Enhancing the Performance of Polymer Solar Cells

https://dx.doi.org/10.1021/acs.jpca.0c02572
J. Phys. Chem. A XXXX, XXX, XXX−XXX

Via Core Engineering of NIR-Absorbing Electron Acceptors. *Adv. Mater.* **2018**, *30*, 1706571.
(34) Li, T.; Dai, S.; Ke, Z.; Yang, L.; Wang, J.; Yan, C.; Ma, W.; Zhan, X. Fused Tris(Thienothiophene)-Based Electron Acceptor with Strong near-Infrared Absorption for High-Performance as-Cast Solar Cells. *Adv. Mater.* **2018**, *30*, 1705969.
(35) Katan, C.; Tretiak, S.; Werts, M. H. V.; Bain, A. J.; Marsh, R. J.; Leonczek, N.; Nicolaou, N.; Badaeva, E.; Mongin, O.; Blanchard-Desce, M. Two-Photon Transitions in Quadrupolar and Branched Chromophores: Experiment and Theory. *J. Phys. Chem. B* **2007**, *111*, 9468−9483.
(36) Delgado, M. C. R.; Kim, E.-G.; Filho, D. A. d. S.; Bredas, J.-L. Tuning the Charge-Transport Parameters of Perylene Diimide Single Crystals Via End and/or Core Functionalization: A Density Functional Theory Investigation. *J. Am. Chem. Soc.* **2010**, *132*, 3375−3387.
(37) Sheik-Bahae, M.; Said, A. A.; Wei, T. H.; Hagan, D. J.; Van Stryland, E. W. Sensitive Measurement of Optical Nonlinearities Using a Single Beam. *IEEE J. Quantum Electron.* **1990**, *26*, 760−769.
(38) Jia, B.; Dai, S.; Ke, Z.; Yan, C.; Ma, W.; Zhan, X. Breaking 10% Efficiency in Semitransparent Solar Cells with Fused-Undecacyclic Electron Acceptor. *Chem. Mater.* **2018**, *30*, 239−245.
(39) Cao, H.; Bauer, N.; Pang, C.; Rech, J.; You, W.; Rupar, P. A. End-Cap Group Engineering of a Small Molecule Non-Fullerene Acceptor: The Influence of Benzothiophene Dioxide. *ACS Appl. Energy Mater.* **2018**, *1*, 7146−7152.
(40) Bonneau, R.; Carmichael, I.; Hug, G. L. Molar Absorption Coefficients of Transient Species in Solution. *Pure Appl. Chem.* **1991**, *63*, 289.
(41) Negres, R. A.; Hales, J. M.; Kobyakov, A.; Hagan, D. J.; Van Stryland, E. W. Experiment and Analysis of Two-Photon Absorption Spectroscopy Using a White-Light Continuum Probe. *IEEE J. Quantum Electron.* **2002**, *38*, 1205−1216.
(42) Said, A. A.; Wamsley, C.; Hagan, D. J.; Van Stryland, E. W.; Reinhardt, B. A.; Roderer, P.; Dillard, A. G. Third- and Fifth-Order Optical Nonlinearities in Organic Materials. *Chem. Phys. Lett.* **1994**, *228*, 646−650.
(43) Lou, A. J. T.; Benis, S.; Gao, M.; Baev, A.; Kim, D.; Van Stryland, E. W.; Hagan, D. J.; Marks, T. J. Third- and Fifth-Order Nonlinear Optical Response of a TICT/Stilbene Hybrid Chromophore. *J. Phys. Chem. C* **2020**, *124*, 5363−5370.
(44) Kirkpatrick, S.; Sutherland, R. L. In *Handbook of Nonlinear Optics*, 2nd ed.; Marcel Dekker, Inc.: New York, 2003; p 689.
(45) Wang, J.; Zhang, J.; Xiao, Y.; Xiao, T.; Zhu, R.; Yan, C.; Fu, Y.; Lu, G.; Lu, X.; Marder, S. R.; et al. Effect of Isomerization on High-Performance Nonfullerene Electron Acceptors. *J. Am. Chem. Soc.* **2018**, *140*, 9140−9147.
(46) The molecules examined here have nominal C_{2h} symmetry. In this point group, all excited states are either 1PA- or 2PA-allowed and (as for all centrosymmetric point groups) 1PA-allowed states are 2PA-forbidden and 2PA-allowed states are 1PA-forbidden.
(47) Padilha, L. A.; Webster, S.; Przhonska, O. V.; Hu, H.; Peceli, D.; Ensley, T. R.; Bondar, M. V.; Gerasov, A. O.; Kovtun, Y. P.; Shandura, M. P.; et al. Efficient Two-Photon Absorbing Acceptor-π-Acceptor Polymethine Dyes. *J. Phys. Chem. A* **2010**, *114*, 6493−6501.
(48) Zheng, S.; Leclercq, A.; Fu, J.; Beverina, L.; Padilha, L. A.; Zojer, E.; Schmidt, K.; Barlow, S.; Luo, J.; Jiang, S.-H.; et al. Two-Photon Absorption in Quadrupolar Bis(acceptor)-Terminated Chromophores with Electron-Rich Bis(heterocycle)vinylene Bridges. *Chem. Mater.* **2007**, *19*, 432−442.
(49) Rumi, M.; Ehrlich, J. E.; Heikal, A. A.; Perry, J. W.; Barlow, S.; Hu, Z.; McCord-Maughon, D.; Parker, T. C.; Röckel, H.; Thayumanavan, S.; et al. Structure−Property Relationships for Two-Photon Absorbing Chromophores: Bis-Donor Diphenylpolyene and Bis(styryl)benzene Derivatives. *J. Am. Chem. Soc.* **2000**, *122*, 9500−9510.
(50) Fu, J.; Padilha, L. A.; Hagan, D. J.; Van Stryland, E. W.; Przhonska, O. V.; Bondar, M. V.; Slominsky, Y. L.; Kachkovski, A. D. Experimental and Theoretical Approaches to Understanding Two-Photon Absorption Spectra in Polymethine and Squaraine Molecules. *J. Opt. Soc. Am. B* **2007**, *24*, 67−76.
(51) Kim, O.-K.; Lee, K.-S.; Woo, H. Y.; Kim, K.-S.; He, G. S.; Swiatkiewicz, J.; Prasad, P. N. New Class of Two-Photon-Absorbing Chromophores Based on Dithienothiophene. *Chem. Mater.* **2000**, *12*, 284−286.
(52) Wang, C.-K.; Macak, P.; Luo, Y.; Ågren, H. Effects of π Centers and Symmetry on Two-Photon Absorption Cross Sections of Organic Chromophores. *J. Chem. Phys.* **2001**, *114*, 9813−9820.
(53) Breitung, E. M.; Shu, C.-F.; McMahon, R. J. Thiazole and Thiophene Analogues of Donor−Acceptor Stilbenes: Molecular Hyperpolarizabilities and Structure−Property Relationships. *J. Am. Chem. Soc.* **2000**, *122*, 1154−1160.
(54) Velusamy, M.; Shen, J.-Y.; Lin, J. T.; Lin, Y.-C.; Hsieh, C.-C.; Lai, C.-H.; Lai, C.-W.; Ho, M.-L.; Chen, Y.-C.; Chou, P.-T.; et al. A New Series of Quadrupolar Type Two-Photon Absorption Chromophores Bearing 11,12-Dibutoxydibenzo[*a*,*c*]-Phenazine Bridged Amines; Their Applications in Two-Photon Fluorescence Imaging and Two-Photon Photodynamic Therapy. *Adv. Funct. Mater.* **2009**, *19*, 2388−2397.
(55) Ricci, F.; Carlotti, B.; Keller, B.; Bonaccorso, C.; Fortuna, C. G.; Goodson, T.; Elisei, F.; Spalletti, A. Enhancement of Two-Photon Absorption Parallels Intramolecular Charge-Transfer Efficiency in Quadrupolar Versus Dipolar Cationic Chromophores. *J. Phys. Chem. C* **2017**, *121*, 3987−4001.
(56) Klikar, M.; le Poul, P.; Růžička, A.; Pytela, O.; Barsella, A.; Dorkenoo, K. D.; Robin-le Guen, F.; Bureš, F.; Achelle, S. Dipolar NLO Chromophores Bearing Diazine Rings as π-Conjugated Linkers. *J. Org. Chem.* **2017**, *82*, 9435−9451.
(57) Ohira, S.; Rudra, I.; Schmidt, K.; Barlow, S.; Chung, S.-J.; Zhang, Q.; Matichak, J.; Marder, S. R.; Brédas, J.-L. Electronic and Vibronic Contributions to Two-Photon Absorption in Donor−Acceptor−Donor Squaraine Chromophores. *Chem. - Eur. J.* **2008**, *14*, 11082−11091.
(58) The generic label "S_n" assigned to the final state of the higher-energy transition $S_1 \rightarrow S_n$ is due to the possibility that this state might reach S_4 or S_5 based on uncertainty in the energetics of these states when comparing ND2PA, TA, and 1PA spectra.
(59) Chung, S.-J.; Rumi, M.; Alain, V.; Barlow, S.; Perry, J. W.; Marder, S. R. Strong, Low-Energy Two-Photon Absorption in Extended Amine-Terminated Cyano-Substituted Phenylenevinylene Oligomers. *J. Am. Chem. Soc.* **2005**, *127*, 10844−10845.
(60) Belfield, K. D.; Morales, A. R.; Hales, J. M.; Hagan, D. J.; Van Stryland, E. W.; Chapela, V. M.; Percino, J. Linear and Two-Photon Photophysical Properties of a Series of Symmetrical Diphenylamino-fluorenes. *Chem. Mater.* **2004**, *16*, 2267−2273.

https://dx.doi.org/10.1021/acs.jpca.0c02572
J. Phys. Chem. A XXXX, XXX, XXX−XXX